


Article

Fabrication of Mg Coating on PEEK and Antibacterial Evaluation for Bone Application

Yang Ji ¹, Xiaoming Yu ^{2,3}  and Hao Zhu ^{1,*}

¹ Department of Stomatology, General Hospital of Northern Theater Command, Shenyang 110016, China; yangji2080@163.com

² School of Material Science and Engineering, Shenyang Ligong University, Shenyang 110159, China; xmyu@sylu.edu.cn

³ Institute of Metal Research, Chinese Academy of Sciences, Shenyang 110016, China

* Correspondence: haozhu2000@163.com; Tel.: +86-024-2885-1331

Abstract: Polyetheretherketone (PEEK) is an alternative biomedical polymer material to traditional metal and ceramic biomaterials. However, as a bioinert material, its wide application in the medical field is seriously restricted due to its lack of bioactivity. In this research, pure Mg was successfully deposited on a PEEK substrate by vapor deposition to improve the antibacterial properties of PEEK implants. The morphology and elemental composition of the coating were characterized by scanning electron microscopy (SEM) and energy-dispersive spectroscopy (EDS). The higher the deposition temperature, the larger the Mg particle size. The Mg coating possesses a hydrophilic surface and a higher surface free energy that create its good biocompatibility. The Mg coating on a PEEK substrate withstands up to 56 days' immersion. The antibacterial test showed that the antibacterial rate of coated PEEK is 99%. Mg-coated PEEK demonstrates promising antibacterial properties.



Citation: Ji, Y.; Yu, X.; Zhu, H. Fabrication of Mg Coating on PEEK and Antibacterial Evaluation for Bone Application. *Coatings* **2021**, *11*, 1010. <https://doi.org/10.3390/coatings11081010>

Academic Editors:
Alexandra Muñoz-Bonilla and Ajay Vikram Singh

Received: 11 July 2021
Accepted: 18 August 2021
Published: 23 August 2021

Publisher's Note: MDPI stays neutral with regard to jurisdictional claims in published maps and institutional affiliations.



Copyright: © 2021 by the authors. Licensee MDPI, Basel, Switzerland. This article is an open access article distributed under the terms and conditions of the Creative Commons Attribution (CC BY) license (<https://creativecommons.org/licenses/by/4.0/>).

Keywords: PEEK; Mg; coating; vapor deposition; antibacterial

1. Introduction

As an alternative biomedical polymer material, polyetheretherketone (PEEK) is easy to process, possesses good biocompatibility, and has a similar Young's modulus to human bone. It is regarded as one of the most promising candidates for spinal, trauma, oral implantology, and orthopedic applications [1–5]. At the same time, PEEK has good X-ray transmission, and can be used with common diagnostical techniques such as X-ray, CT, and MRI, making it popular. Pace et al. [6] successfully implanted a composite CF/PEEK cup into the human body. After 28 months' implantation, histological analysis showed that the maximum wear depth was 0.130 mm, and only a small amount of wear particles entered the periprosthetic tissues. The possibility of using PEEK for dental implants was also confirmed through static compression experiments of various PEEK-based composites. Because of the introduction of fibers, the mechanical properties of PEEK were enhanced; even 4 mm diameter samples were able to meet the requirements of implantation [7]. However, PEEK is a type of bioinert material that induces poor bonding with peripheral tissue, resulting in aseptic loosening and even implantation failure [8]. Therefore, improvement in the bioactivity for PEEK material is needed. Surface modification is an effective method that is widely used with biomedical materials. In previous studies, surface bioactivity was enhanced via appropriate surface modification methods, while preserving the original mechanical properties.

As an example of a commonly used orthopedic bioactive material, hydroxyapatite (HA) was applied to form PEEK composites, and was shown to improve the bioactivity [9–11]. Nevertheless, the poor physical bonding between HA and PEEK compromises the mechanical properties. Reduced graphene oxide (rGo) was combined with PEEK,

and different porous lattice structures were produced to improve interface biocompatibility and mimic bone [12]. Various materials such as TiO₂ [13–15], Ti [16,17], Ta [18,19], and carbon nanotubes [20] have also been deposited on PEEK to improve biocompatibility. Postoperative bacterial infection, a common complication, is still hindering patient recovery, even causing surgical failures, which is a serious problem requiring a solution. The basic requirements for an ideal orthopedic material are bone bioactivity and antibacterial properties.

Nowadays, magnesium (Mg) and Mg alloys have attracted much attention because of their excellent bioactivity [21–24] and suitable biodegradability [25,26]. Furthermore, the anti-tumor [27–29] and antibacterial abilities [30–34] have also been widely investigated. The Mg²⁺ released from the degradation of a Mg implant possesses osteogenic and angiogenic abilities, while its antibacterial properties originate from the alkaline degradation environment. As a result, Mg-based metals have gradually shown promise as candidates for medical applications. Mg alloys in the form of bulk materials such as bone screws and plates have been widely investigated, and there are already two existing examples of successful Mg-alloy-based orthopedic products [24–26]. Mg-based products were used to mend fractures of metacarpals and phalanges. Nevertheless, due to their relatively low tensile strength, Mg alloys cannot be applied in load-bearing positions. In order to fully utilize bioactive Mg alloys, their coating was fabricated on medical materials [35]. The possibility of using Mg coating as an orthopedics material was confirmed. Because of galvanic corrosion, the degradation rate of Mg coating on Ti alloys increases [35]. In contrast, pure Mg can improve corrosion resistance [36,37]. As a result, pure Mg can be coated on bioinert materials such as PEEK to improve their surface bioactivity. Pure Mg film was deposited on Si wafer [38] and porous Ti6Al4V scaffolds [39], and the bioactivity of the substrate was improved owing to the Mg coating.

In this study, high-purity Mg was deposited on a PEEK substrate by vacuum evaporation, which was expected to reduce bacterial infection. This may be a new way to improve the bioactivity of PEEK for medical applications.

2. Materials and Methods

2.1. Materials and Coating

Mg coating was applied on a PEEK substrate by vacuum evaporation. A schematic illustration of the furnace used is shown in Figure 1. High-purity (99.99 wt %) Mg was placed in a graphite crucible and evaporated. The working pressure was set to 0.1 Pa; Mg powder was evaporated at 500 °C; deposition temperatures were set to 150, 170, 190, and 210 °C; and the deposition time was 30 min. Commercial-grade medical PEEK plates, 16 × 2 mm each, were used as substrates. The PEEK substrates were sand blasted to create a rough surface to strengthen the mechanical combination of Mg coating and substrates. Then, the substrates were ultrasonically cleaned in acetone and deionized water, blown dry by N₂ gas, and then placed in the deposition zone at setting temperature. The generated Mg vapor was transported by high-purity Ar gas flow and spontaneously condensed on the PEEK substrates inside the deposition chamber. The surface morphology of the coating was observed using a scanning electron microscope (SEM, JSM-6460; JEOL, Tokyo, Japan) equipped with an energy-dispersive X-ray analyzer (EDX; Oxford, UK). X-ray diffraction (XRD, D/Max-2500PC, Rigaku, Tokyo, Japan) was used to investigate the crystallographic structure of the deposited coatings. A laser scanning confocal microscope (LSCM, LEXT laser microscope OLS 4000, Olympus, Tokyo, Japan) was employed to investigate the surface roughness. The hydrophilicity of the coated and uncoated samples was characterized by static contact angles.

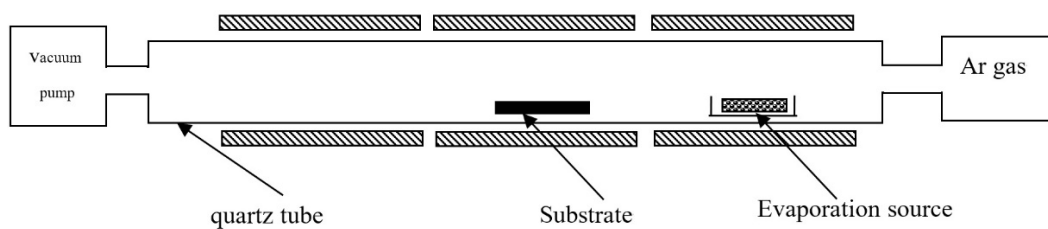


Figure 1. Schematic illustration of furnace used for deposition.

2.2. Immersion Test

The Mg coating on PEEK samples was subjected to an immersion test in Hank's solution at 37 ± 0.5 °C with an extraction ratio of $1.25 \text{ cm}^2/\text{mL}$ up to 56 days, and the Hank's solution was refreshed every day. The degradation product of the Mg coating was alkaline, so the pH value could be used as an indicator of degradation. Therefore, the pH values of the Hank's solution were monitored.

2.3. Antibacterial Test

PEEK substrates and pure Mg coating were cultured with a *Staphylococcus aureus* (*S. aureus*) suspension, which is the most common bacteria that causes postoperative infection, prepared in a sterilized PBS solution with a ratio of $1.25 \text{ cm}^2/\text{mL}$, and then samples were incubated at 37 ± 0.5 °C for 6, 12, and 24 h. The co-cultured bacterial suspensions were diluted to $(1-2) \times 10^3 \text{ CFU}/\text{mL}$. We added 0.1 mL of the diluted bacterial suspension onto the nutrition agar plate and spread it evenly, which was incubated again at 37 ± 0.5 °C for another 24 h, and then the bacterial colonies were counted. The antibacterial efficacy (ABE) was calculated using the following equation:

$$ABE \% = \frac{N_b - N_t}{N_b} \times 100 \quad (1)$$

where N_b and N_t are the numbers of viable bacterial colonies of the uncoated PEEK and the coated PEEK, respectively.

3. Results and Discussion

3.1. Morphology of the Mg Coating

Because of the relatively high saturated vapor pressure of Mg, Mg was likely to sublime below its melting point. Considering the ultimate pressure of our apparatus, the working pressure was set to 1×10^{-1} Pa. The vapor pressure of pure Mg is around 1×10^{-1} Pa at about 439 °C; thus, the evaporation temperature was set to 500 °C in order to obtain sufficient vapor pressure. The evaporation temperature, working pressure, and substrate temperature determined the final surface quality of the Mg coating. Among them, substrate temperature was the most critical factor. Therefore, the dependence of the surface quality of the Mg coating on substrate temperature was investigated in this study. The thickness of the Mg coating was about 100 μm . The surface morphology of the Mg coating at different substrate temperatures of 150, 170, 190, and 210 °C is shown in Figure 2. The Mg coatings fully covered the PEEK substrates and consisted of various sizes of particles. It can be seen that the coatings were uniform, but loose. The EDS analysis showed that the coatings were pure Mg, as shown in Figure 2e. According to the XRD results (Figure 3), pure Mg was observed on the surfaces of the PEEK substrates and there were few differences between the samples. The size of the particles increased with the increase in substrate temperature. The particle size was about 1–4 μm at 150 °C, as shown in Figure 2a. The size of the particles sharply increased at 170 °C, and the particles were in the shape of strips. Due to low substrate temperature, diffusion of Mg was not significant. Therefore, the particles grew on their own. As is well known, Mg possess a hexagonal structure. We predicted that the growth rate along the c axis would be higher than that of the a and b axes. As a result, particles increasingly lengthened as

shown in Figure 2b. With the temperature increased to 190 °C, the particle size increased to 20–30 μm. The particles were diffused, combined with adjacent particles, and thus grew larger. As shown in Figure 2d, there was no further obvious change in particle shape, only the size slightly increased. Atsushi et al. [40] obtained a similar result at around 210 °C, and with higher substrate temperatures [40] than this experiment, the gaps between particles were smaller and particles tended to fuse with adjacent ones. However, the different particle size could affect the degradation rate of the Mg coating. At the same time, the grooves between particles were easily filled with corrosive liquid, causing the degradation rate to simultaneously increase.

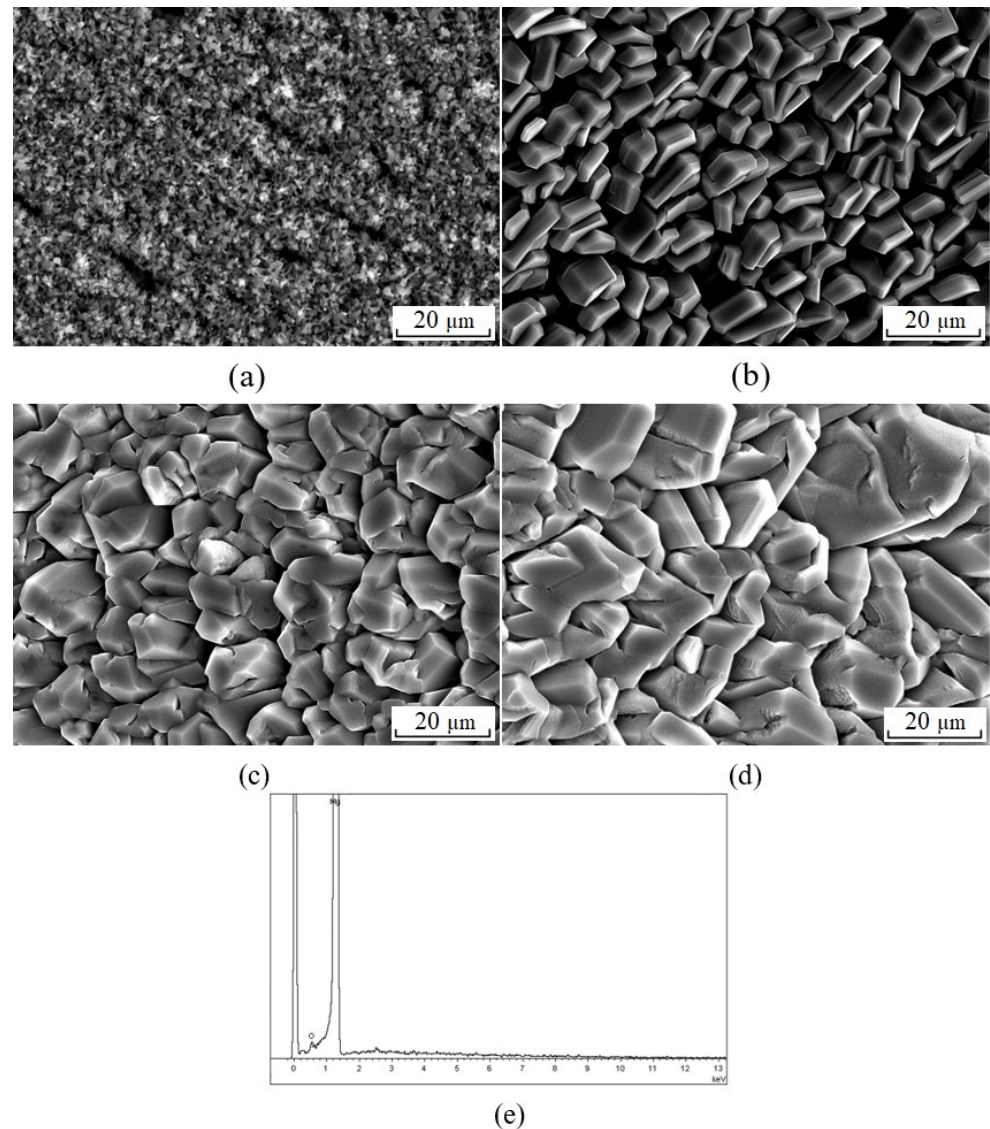


Figure 2. Surface morphologies of Mg coating at different substrate temperatures: (a) 150 °C, (b) 170 °C, (c) 190 °C, and (d) 210 °C; and (e) EDS analysis.

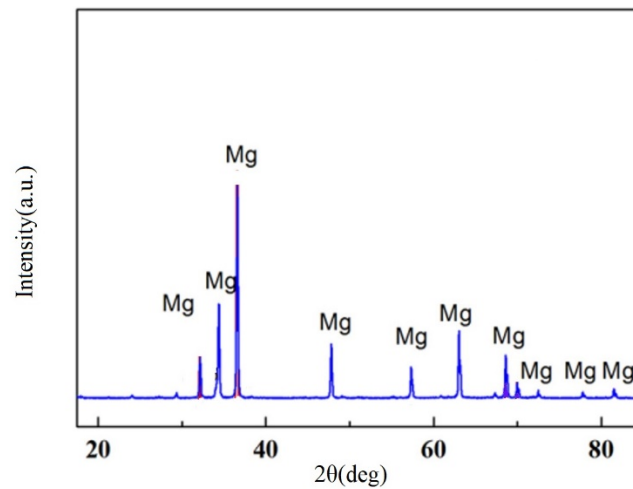


Figure 3. XRD pattern of Mg coating on a PEEK substrate.

3.2. Surface Roughness of the Mg Coating and the PEEK Substrate

For implantable biomaterials, surface topography is crucial because it affects the response of the immune system [41]. Material surface properties such as roughness and wettability play a paramount role in cell adhesion, cell proliferation, osteointegration, and implant stability [42]. Therefore, a laser scanning confocal microscope (LSCM) was adopted to investigate the surface roughness of the Mg coating. As shown in Figure 2b, the surface was too loose and the gaps between particles were large enough to allow the deposition of excessive corrosive liquid, causing the degradation rate to increase correspondingly. The samples deposited at 190 or 210 °C (Figure 2c,d) obtained better density results. Therefore, surface roughness was investigated on samples at 210 °C. The LSCM images are shown in Figure 4. Compared to PEEK substrates, the surface roughness of Mg coatings was much higher at 12.1 μm, with only 4.2 μm for the PEEK substrates. The rough surface was beneficial for the attachment of cells and growth of tissue. However, a roughness that is too high can increase the size of the contact surface with the solution. An appropriate surface roughness can limit the degradation rate. Consequently, the bioactivity of the Mg coating was strongly restricted by the degradation process.

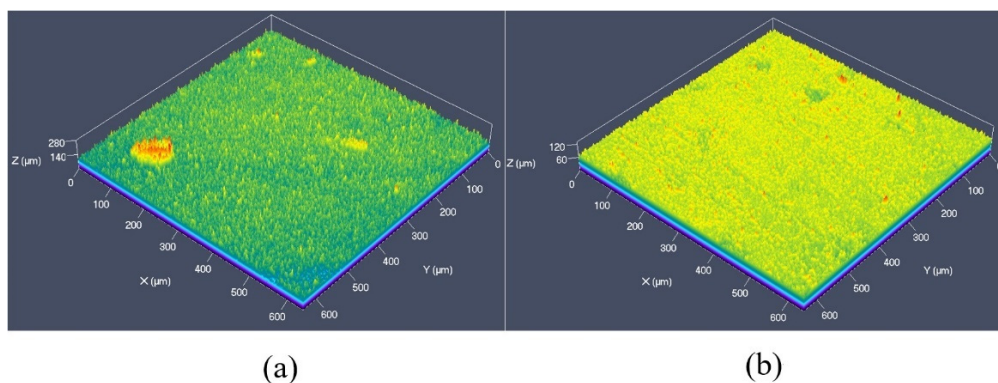


Figure 4. LSCM images: (a) Mg coating; (b) PEEK substrate.

3.3. Wettability and Surface Free Energy of Mg Coating

As an implanted biomaterial, surface properties are critical to determine their biocompatibility and bioactivity. Particularly due to its reaction with H₂O, the degradation behavior of Mg coating is strongly affected by surface quality. As is well-known, its overly rapid degradation rate has restricted the wide application of Mg in medicine. Various surface modification methods have been attempted to control the degradation of Mg. Uniform

and denser surfaces mean a longer degradation period. Hydrophobic surfaces also decrease the degradation rate of Mg. However, hydrophilic surfaces are optimal for implantable material; therefore, wettability is an important evaluation factor for biomaterials.

The hydrophilicity of the Mg coating and the PEEK substrate was characterized by static contact angles. Experiments, with samples deposited at 210 °C, were conducted by a static contact angles test. Figure 5 reveals that the Mg coating had a hydrophilic surface with a contact angle of 51°, while that of PEEK was 121°, which means that the Mg coating provided a significant improvement in hydrophilic characteristics. The surface energy was also calculated from the contact angle measurements. Double-distilled water and α -BrNp were used for the contact angle measurement according to the following formula [43]:

$$\begin{cases} \gamma_{L1}(1 + \cos \theta_1) = 2\sqrt{\gamma_s^d \gamma_{L1}^d} + 2\sqrt{\gamma_s^p \gamma_{L1}^p} \\ \gamma_{L2}(1 + \cos \theta_2) = 2\sqrt{\gamma_s^d \gamma_{L2}^d} + 2\sqrt{\gamma_s^p \gamma_{L2}^p} \end{cases} \quad (2)$$

where θ is the contact angle; γ_L , γ_L^p , and γ_L^d are the interface energy, and polar and dispersive components of the liquid phase, respectively; and γ_s , γ_s^p , and γ_s^d are the surface energy, and polar and dispersive components of the solid phase, respectively. By measuring the contact angles of the two different fluids with known γ_L^p and γ_L^d , Equation (2) could be solved to obtain the γ_s^p and γ_s^d of the surface energy of the Mg coating. The surface energy γ_s of Mg coating was 52.45 mN·m⁻¹, which is higher than that of the PEEK substrate (7.37 mN·m⁻¹). The low water contact angle of the Mg coating resulted in the strong spreadability of the surface, whereby the cells could spread completely over the substrate surface. It was found that cell spreading was dependent on the polar component of surface energy (γ_s^p) [44], which was even higher for the Mg coating (12.25 mN·m⁻¹) than that of PEEK (1.71 mN·m⁻¹). The surface free energy was found to have a strong correlation with alkaline phosphatase activity [44]. Biocompatibility of the Mg coating benefited from the hydrophilic surface and higher surface free energy.

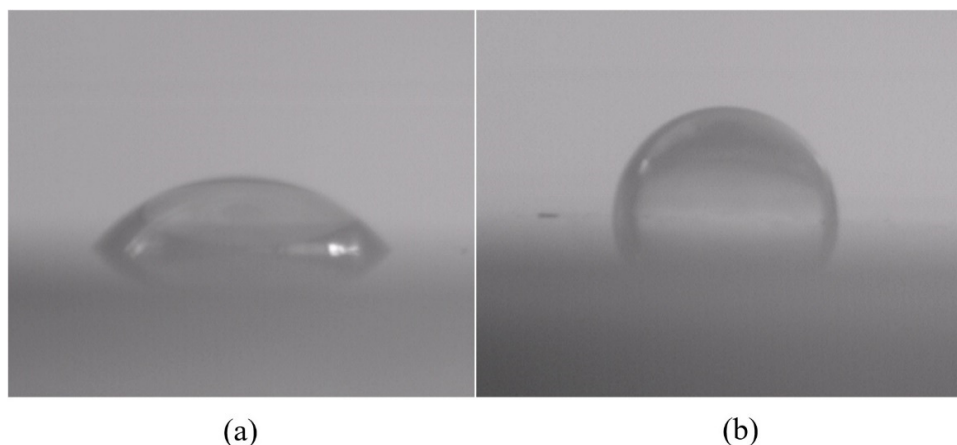


Figure 5. Contact angles of samples with water: (a) Mg coating; (b) PEEK substrate.

3.4. Degradation Behavior of Mg Coating

Because of the metastable state of most coatings, the properties of the coating are normally different from those of bulk. In particular, the surface of the Mg coating was not dense when fabricated by vapor deposition. The bioactivity of Mg was demonstrated through the degradation process. Therefore, we needed to investigate the degradation behavior of the Mg coating. The degradation product of Mg was alkaline, so the monitoring of the variation in the pH value is used to demonstrate the degradation process. Figure 6 shows the curve of changes to the pH of Hank's solution immersed with Mg coating with different substrate temperatures. A higher pH value represents a higher degradation rate. At first, the pH value of the leaching solution increased to 11 for all samples. The pH

value then slowly decreased to 10 over the next 7 days. Over the following 5 weeks, the pH value for all samples slightly decreased and remained steady between 9.5 and 10. After 35 days, the pH value dropped to 8 for samples with substrate temperatures of 150 and 170 °C. A possible reason for this finding is that the solution penetrated into the gaps between coating and substrate and the coating began to peel off from the surface of substrate. The trend for the other samples was nearly the same: samples of 190 °C persisted for 49 days and samples of 210 °C persisted for 56 days. All the Mg coatings completely vanished after 56 days for all samples. With higher substrate temperature, the coating was denser, as shown in Figure 2. Due to the gaps between particles, contact area with the solution was larger, which increased the degradation rate. The surface of the sample deposited at 210 °C was denser than the others, so it lasted 56 days. We determined that 210 °C is an optimal deposition temperature for the relatively long-term implant.

Compared to the Mg-coated Ti6Al4V alloy applied by arc ion plating method, the degradation rate of the Mg coating on PEEK is lower [35]. The Mg coating on the Ti alloy substrate vanished after 2 weeks, with the Mg coating on PEEK only after 8 weeks. Although the surface was denser for the Mg coating on the Ti alloy substrate, no galvanic corrosion took place for the Mg coating on PEEK. Therefore, the degradation rate was much lower, and the Mg coating on PEEK seems more suitable for long term reconstruction of bone.

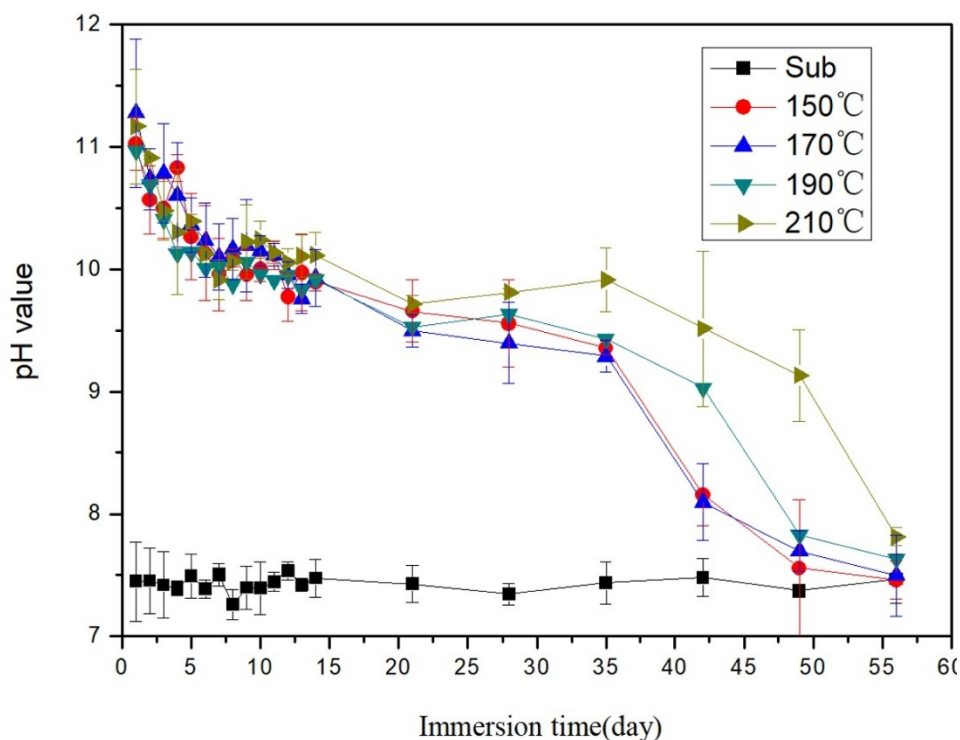


Figure 6. pH changes in Hank's solution immersed with Mg-coated samples with different substrate temperatures.

3.5. Antibacterial Properties of Mg Coating

As is known, postoperative infections, as serious complications, seriously slow recovery for patients. Therefore, intrinsic antibacterial properties for bone implants are highly desirable. The antibacterial properties of Mg originate from alkaline degradation products. Therefore, we hoped that the Mg coating on PEEK can provide satisfactory antibacterial properties. Figure 7 shows the antibacterial effects of PEEK substrates and Mg coating co-cultured with *S. aureus* at 37 °C for 6, 12, and 24 h. After co-culturing for 6 h, there were more bacteria on the sample cultured with the PEEK substrate, while there were less bacterial colonies on the Mg-coated sample. After co-culturing for 12 h, the number

of bacterial colonies increased for the PEEK sample, while there were only two bacterial colonies for the Mg-coated sample. As for after 24 h, there was no obvious change in the PEEK group, and bacteria completely vanished from the Mg-coated sample. PEEK was shown to be a type of bio-inert material without any antibacterial properties. Most of the bacteria that typically cause orthopedic infections such as *S. aureus* cannot survive in strong alkaline environments with the degradation of Mg coating. The antibacterial rate of the Mg-coated sample was 78% for 6 h. When co-cultured for 12 and 24 h, the antibacterial rate reached 99%. During the whole degradation period of the Mg-coated sample, the pH was kept at a relatively high level to maintain consistent antibacterial properties until the complete degradation of the Mg coating.

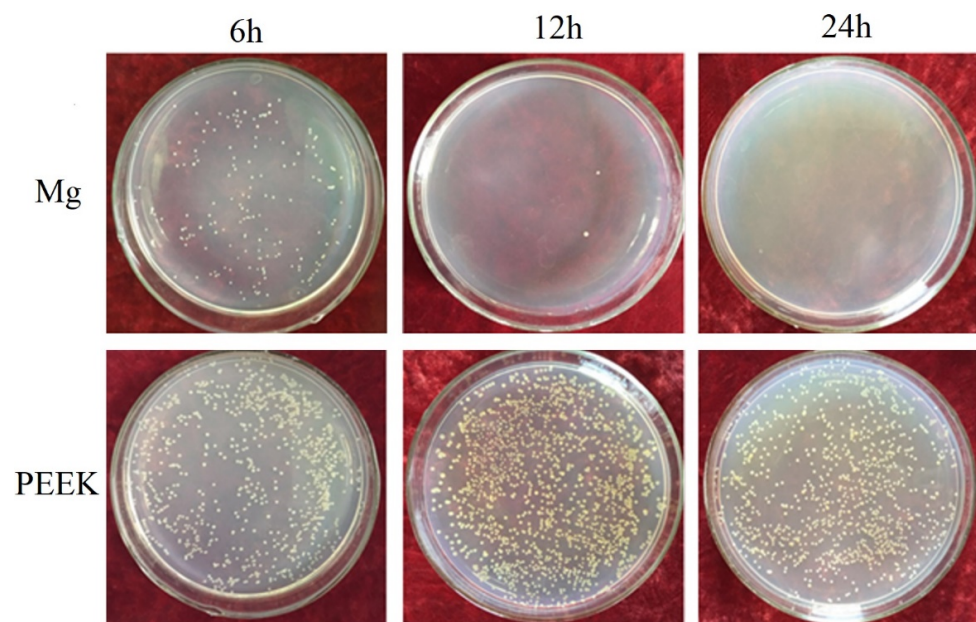


Figure 7. Antibacterial effects of PEEK with and without Mg coating co-cultured with *S. aureus* at 37 °C for 6, 12, and 24 h.

4. Conclusions

In this study, pure Mg was coated on PEEK substrates by vapor deposition. The Mg coating was uniform and relatively dense at a substrate temperature of 210 °C. The hydrophilic surface and higher surface free energy of the Mg coating were found to be useful in improving its biocompatibility. The Mg coating completely degraded after 56 days of immersion in Hank's solution. The Mg coating exhibited satisfactory antibacterial properties with an antibacterial rate of 99%. By the vapor deposition method, a biofunctional Mg coating may be applied on various bio-inert medical materials to improve their bioactivities.

Author Contributions: Conceptualization, X.Y. and H.Z.; methodology, Y.J.; validation, Y.J., X.Y., and H.Z.; formal analysis, Y.J. and X.Y.; investigation, Y.J. and X.Y.; resources, Y.J. and X.Y.; data curation, Y.J. and X.Y.; writing—original draft preparation, Y.J., X.Y.; writing—review and editing, H.Z.; supervision, H.Z.; project administration, X.Y. and H.Z.; funding acquisition, X.Y. and H.Z. All authors have read and agreed to the published version of the manuscript.

Funding: This research was funded by the Natural Science Foundation of Liaoning Province of China (No. 20180551105 and No. 2019-MS-326); and research funding for talent introduction by Shenyang Ligong University (No.101047000826).

Institutional Review Board Statement: Not applicable.

Informed Consent Statement: Not applicable.

Data Availability Statement: Not applicable.

Conflicts of Interest: The authors declare no conflict of interest. The funders had no role in the design of the study; in the collection, analyses, or interpretation of data; in the writing of the manuscript, or in the decision to publish the results.

References

1. Kurtz, S.M.; Devine, J.N. PEEK biomaterials in trauma, orthopedic, and spinal implants. *Biomaterials* **2007**, *28*, 4845–4869. [[CrossRef](#)] [[PubMed](#)]
2. Li, S.; Wang, T.; Hu, J.; Li, Z.; Wang, B.; Wang, L.; Zhou, Z. Surface porous poly-ether-ether-ketone based on three-dimensional printing for load-bearing orthopedic implant. *J. Mech. Behav. Biomed. Mater.* **2021**, *120*, 104561. [[CrossRef](#)]
3. Gao, C.; Wang, Z.; Jiao, Z.; Wu, Z.; Guo, M.; Wang, Y.; Liu, J.; Zhang, P. Enhancing antibacterial capability and osseointegration of polyetheretherketone (PEEK) implants by dual-functional surface modification. *Mater. Des.* **2021**, *205*, 109733. [[CrossRef](#)]
4. Haleem, A.; Javaid, M. Polyether ether ketone (PEEK) and its 3D printed implants applications in medical field: An overview. *Clin. Epidemiol. Glob. Health* **2019**, *7*, 571–577. [[CrossRef](#)]
5. Oladapo, B.I.; Zahedi, S.A.; Ismail, S.O.; Omigbodun, F.T. 3D printing of PEEK and its composite to increase biointerfaces as a biomedical material- A review. *Colloids Surf. B Biointerfaces* **2021**, *203*, 111726. [[CrossRef](#)]
6. Pace, N.; Marinelli, M.; Spurio, S. Technical and Histologic Analysis of a Retrieved Carbon Fiber–Reinforced Poly-Ether-Ether-Ketone Composite Alumina-Bearing Liner 28 Months after Implantation. *J. Arthroplast.* **2008**, *23*, 151–155. [[CrossRef](#)]
7. Schwitalla, A.D.; Spintig, T.; Kallage, I.; Müller, W.D. Pressure behavior of different PEEK materials for dental implants. *J. Mech. Behav. Biomed. Mater.* **2016**, *54*, 295–304. [[CrossRef](#)]
8. Wu, X.; Liu, X.; Wei, J.; Ma, J.; Deng, F.; Wei, S. Nano-TiO₂/PEEK bioactive composite as a bone substitute material: In vitro and in vivo studies. *Int. J. Nanomed.* **2012**, *7*, 1215–1225.
9. Yu, S.; Hariram, K.P.; Kumar, R.; Cheang, P.; Aik, K.K. In vitro apatite formation and its growth kinetics on hydroxyapatite/polyetheretherketone biocomposites. *Biomaterials* **2005**, *26*, 2343–2352. [[CrossRef](#)]
10. Manzoor, F.; Golbang, A.; Jindal, S.; Dixon, D.; McIlhagger, A.; Harkin-Jones, E.; Crawford, D.; Mancuso, E. 3D printed PEEK/HA composites for bone tissue engineering applications: Effect of material formulation on mechanical performance and bioactive potential. *J. Mech. Behav. Biomed. Mater.* **2021**, *121*, 104601. [[CrossRef](#)]
11. Ma, H.; Suonan, A.; Zhou, J.; Yuan, Q.; Liu, L.; Zhao, X.; Lou, X.; Yang, C.; Li, D.; Zhang, Y.G. PEEK (Polyether-ether-ketone) and its composite materials in orthopedic implantation. *Arab. J. Chem.* **2021**, *14*, 102977. [[CrossRef](#)]
12. Oladapo, B.I.; Zahedi, S.A. Improving bioactivity and strength of PEEK composite polymer for bone application. *Mater. Chem. Phys.* **2021**, *266*, 124485. [[CrossRef](#)]
13. Lu, T.; Liu, X.; Qian, S.; Cao, H.; Qiao, Y.; Mei, Y.; Chu, P.K.; Ding, C. Multilevel surface engineering of nanostructured TiO₂ on carbon-fiber-reinforced polyetheretherketone. *Biomaterials* **2014**, *35*, 5731–5740. [[CrossRef](#)]
14. Sargin, F.; Erdogan, G.; Kanbur, K.; Turk, A. Investigation of in vitro behavior of plasma sprayed Ti, TiO₂ and HA coatings on PEEK. *Surf. Coat. Technol.* **2021**, *411*, 126965. [[CrossRef](#)]
15. Xian, P.; Chen, Y.; Gao, S.; Qian, J.; Zhang, W.; Udduttula, A.; Huang, N.; Wan, G. Polydopamine (PDA) mediated nanogranular-structured titanium dioxide (TiO₂) coating on polyetheretherketone (PEEK) for oral and maxillofacial implants application. *Surf. Coat. Technol.* **2020**, *401*, 126282. [[CrossRef](#)]
16. Suska, F.; Omar, O.; Emanuelsson, L.; Taylor, M.; Gruner, P.; Kinbrum, A.; Hunt, D.; Hunt, T.; Taylor, A.; Palmquist, A. Enhancement of CRF-PEEK osseointegration by plasma-sprayed hydroxyapatite: A rabbit model. *J. Biomater. Appl.* **2014**, *29*, 234–242. [[CrossRef](#)]
17. Kashii, M.; Kitaguchi, K.; Makino, T.; Kaito, T. Comparison in the same intervertebral space between titanium-coated and uncoated PEEK cages in lumbar interbody fusion surgery. *J. Orthop. Sci.* **2020**, *25*, 565–570. [[CrossRef](#)] [[PubMed](#)]
18. Lu, T.; Wen, J.; Qian, S.; Cao, H.; Ning, C.; Pan, X.; Jiang, X.; Liu, X.; Chu, P.K. Enhanced osteointegration on tantalum-implanted polyetheretherketone surface with bone-like elastic modulus. *Biomaterials* **2015**, *51*, 173–183. [[CrossRef](#)]
19. Mei, S.; Yang, L.; Pan, Y.; Wang, D.; Wang, X.; Tang, T.; Wei, J. Influences of tantalum pentoxide and surface coarsening on surface roughness, hydrophilicity, surface energy, protein adsorption and cell responses to PEEK based biocomposite. *Colloids Surf. B Biointerfaces* **2019**, *174*, 207–215. [[CrossRef](#)] [[PubMed](#)]
20. Lyu, H.; Jiang, N.; Li, Y.; Zhang, D. Enhancing CF/PEEK interfacial adhesion by modified PEEK grafted with carbon nanotubes. *Compos. Sci. Technol.* **2021**, *210*, 108831. [[CrossRef](#)]
21. Chen, L.; Fu, X.; Pan, H.; Peng, W.; Lei, W.; Tan, L.; Wang, K.; Ying, Z.; Ke, Y.; Chu, P.K. Biodegradable Mg-Cu alloys with enhanced osteogenesis, angiogenesis, and long-lasting antibacterial effects. *Sci. Rep.* **2016**, *6*, 27374.
22. Chen, Z.; Mao, X.; Tan, L.; Friis, T.; Wu, C.; Crawford, R.; Xiao, Y. Osteoimmunomodulatory properties of magnesium scaffolds coated with β -tricalcium phosphate. *Biomaterials* **2014**, *35*, 8553–8565. [[CrossRef](#)]
23. Zhai, Z.; Qu, X.; Li, H.W.; Ke, Y.; Peng, W.; Tan, L.; Ouyang, Z.X.; Liu, X.Q.; Dai, K.R. The effect of metallic magnesium degradation products on osteoclast-induced osteolysis and attenuation of NF- κ B and NFATc1 signaling. *Biomaterials* **2014**, *35*, 6299–6310. [[CrossRef](#)]
24. Cheng, M.Q.; Wahafu, T.; Jiang, G.F.; Liu, W.; Qiao, Y.Q.; Peng, X.C.; Cheng, T.; Zhang, X.L.; He, G.; Liu, X.Y. A novel open-porous magnesium scaffold with controllable microstructures and properties for bone regeneration. *Sci. Rep.* **2016**, *6*, 24134. [[CrossRef](#)] [[PubMed](#)]

25. Zhao, D.; Witte, F.; Lu, F.; Wang, J.; Li, J.; Qin, L. Current status on clinical applications of magnesium-based orthopaedic implants: A review from clinical translational perspective. *Biomaterials* **2016**, *17*, 287–302. [[CrossRef](#)] [[PubMed](#)]
26. Tan, L.; Yu, X.; Wan, P.; Yang, K. Biodegradable Materials for Bone Repairs: A Review. *J. Mater. Sci. Technol.* **2013**, *29*, 503–513. [[CrossRef](#)]
27. Wang, Q.; Jin, S.; Lin, X.; Zhang, Y.; Ren, L.; Yang, K. Cytotoxic Effects of Biodegradation of Pure Mg and MAO-Mg on Tumor Cells of MG63 and KB. *J. Mater. Sci. Technol.* **2014**, *30*, 487–492. [[CrossRef](#)]
28. Qu, X.; Jin, F.; Hao, Y.; Zhu, Z.; Li, H.; Tang, T.; Dai, K. Nonlinear association between magnesium intake and the risk of colorectal cancer. *Eur. J. Gastroenterol. Hepatol.* **2013**, *25*, 309–318. [[CrossRef](#)] [[PubMed](#)]
29. Li, M.; Ren, L.; Li, L.H.; He, P.; Lan, G.B.; Zhang, Y.; Yang, K. Cytotoxic Effect on Osteosarcoma MG-63 Cells by Degradation of Magnesium. *J. Mater. Sci. Technol.* **2014**, *30*, 888–893.
30. Robinson, D.A.; Griffith, R.W.; Dan, S.; Evans, R.B.; Conzemius, M.G. In vitro antibacterial properties of magnesium metal against *Escherichia coli*, *Pseudomonas aeruginosa* and *Staphylococcus aureus*. *Acta Biomater.* **2009**, *6*, 1869–1877. [[CrossRef](#)]
31. Ren, L.; Lin, X.; Tan, L.; Yang, K. Effect of surface coating on antibacterial behavior of magnesium based metals. *Mater. Lett.* **2011**, *65*, 3509–3511. [[CrossRef](#)]
32. Li, Y.; Liu, G.; Zhai, Z.; Liu, L.; Li, H.; Yang, K.; Tan, L.; Wan, P.; Liu, X.; Ouyang, Z. Antibacterial properties of magnesium in an in vitro and in vivo model of implant-associated MRSA infection. *Antimicrob. Agents Chemother.* **2014**, *58*, 7586–7591. [[CrossRef](#)]
33. Cui, L.-Y.; Ji, X.U.; Na, L.U.; Zeng, R.-C.; Zou, Y.H.; Li, S.-Q.; Zhang, F. In vitro corrosion resistance and antibacterial properties of layer-by-layer assembled chitosan/poly-L-glutamic acid coating on AZ31 magnesium alloys. *Trans. Nonferrous Met. Soc. China* **2017**, *27*, 1081–1086. [[CrossRef](#)]
34. Liu, L.; Li, P.; Zou, Y.; Luo, K.; Zhang, F.; Zeng, R.C.; Li, S. In vitro corrosion and antibacterial performance of polysiloxane and poly(acrylic acid)/gentamicin sulfate composite coatings on AZ31 alloy. *Surf. Coat. Technol.* **2016**, *291*, 7–14. [[CrossRef](#)]
35. Yu, X.; Ibrahim, M.; Lu, S.; Yang, H.; Tan, L.; Yang, K. MgCu coating on Ti6Al4V alloy for orthopedic application. *Mater. Lett.* **2018**, *233*, 35–38. [[CrossRef](#)]
36. Fukumoto, S.; Sugahara, K.; Yamamoto, A.; Tsubakino, H. Improvement of corrosion resistance and adhesion of coating layer for magnesium alloy coated with high purity magnesium. *Mater. Trans.* **2003**, *44*, 518–523. [[CrossRef](#)]
37. Tsubakino, H.; Yamamoto, A.; Fukumoto, S.; Watanabe, A.; Sugahara, K.; Inoue, H. High-purity magnesium coating on magnesium alloys by vapor deposition technique for improving corrosion resistance. *Mater. Trans.* **2003**, *44*, 504–510. [[CrossRef](#)]
38. Salunke, P.; Shanov, V.; Witte, F. High purity biodegradable magnesium coating for implant application. *Mater. Sci. Eng. B* **2011**, *176*, 1711–1717. [[CrossRef](#)]
39. Li, X.; Gao, P.; Wan, P.; Pei, Y.; Shi, L.; Fan, B.; Shen, C.; Xiao, X.; Yang, K.; Guo, Z. Novel Bio-functional Magnesium Coating on Porous Ti6Al4V Orthopaedic Implants: In vitro and In vivo Study. *Sci. Rep.* **2017**, *7*, 40755. [[CrossRef](#)] [[PubMed](#)]
40. Yamamoto, A.; Watanabe, A.; Sugahara, K.; Fukumoto, S.; Tsubakino, H. Platform Science and Technology for Advanced Magnesium Alloys. Deposition Coating of Magnesium Alloys with Pure Magnesium. *Mater. Trans.* **2001**, *42*, 1237–1242. [[CrossRef](#)]
41. Abaricia, J.O.; Farzad, N.; Heath, T.J.; Simmons, J.; Morandini, L.; Olivares-Navarrete, R. Control of innate immune response by biomaterial surface topography, energy, and stiffness. *Acta Biomater.* **2021**, *4*, 21. [[CrossRef](#)]
42. Porrelli, D.; Mardirossian, M.; Crapisi, N.; Urban, M.; Ulian, N.A.; Bevilacqua, L.; Turco, G.; Maglione, M. Polyetheretherketone and titanium surface treatments to modify roughness and wettability—Improvement of bioactivity and antibacterial properties. *J. Mater. Sci. Technol.* **2021**, *95*, 213–224. [[CrossRef](#)]
43. Ding Kwok, S.C.H.; Ha, P.C.T.; McKenzie, D.R.; Bilek, M.M.M.; Chu, P.K. Biocompatibility of calcium and phosphorus doped diamond-like carbon thin films synthesized by plasma immersion ion implantation and deposition. *Diam. Relat. Mater.* **2006**, *15*, 893–897. [[CrossRef](#)]
44. Harnett, E.M.; Alderman, J.; Wood, T. The surface energy of various biomaterials coated with adhesion molecules used in cell culture. *Colloids Surf. B Biointerfaces* **2007**, *55*, 90–97. [[CrossRef](#)]